Supplementary Information (SI) for Journal of Materials Chemistry A.
This journal is © The Royal Society of Chemistry 2025

Supplementary Information

Interlayer-stacking mode modulation in an imine covalent organic framework for efficient photocatalytic hydrogen production

Kang-Hua Li,[a,b] Li-Na Liu,[c] Zhong-Xin Xue,[a] Zi-Wen Xu,[a] Yogesh Gawale,[a] Fu-Gang Zhao,[*,d] Wei-Shi Li*[,a,b,c]

[a] State Key Laboratory of Fluorine and Nitrogen Chemistry and Advanced Materials, Shanghai Institute of Organic Chemistry, University of Chinese Academy of Sciences, Chinese Academy of Sciences, 345 Lingling Road, Shanghai 200032, P. R. China. E-mail: liws@mail.sioc.ac.cn

[b] The Education Ministry Key Laboratory of Resource Chemistry, Shanghai Normal University, Shanghai 200234, P. R. China.

[c] Engineering Research Center of Zhengzhou for High Performance Organic Functional Materials, Zhengzhou University of Technology, 6 Yingcai Street, Huiji District, Zhengzhou 450044, P. R. China.

[d] School of Chemistry and Chemical Engineering, Zhejiang Sci-Tech University, Hangzhou 310018, China. E-Mail: fgzhao@zstu.edu.cn

1. Characterization methods

Fourier transform infrared (FT-IR) spectroscopy was performed on Avatar 360 spectrometer using a solid powder sample. Solid-state magic angle spinning ^{13}C NMR was measured on an Agilent 600 DD2 spectrometer while ^{1}H NMR spectrum measurement was conducted on a Varian Mercury 400 spectrometer. Thermogravimetric analysis (TGA) was carried out on a TGA Q500 analysis instrument at a heating rate of 10 °C min^{-1}, covering temperature range from room temperature to 800 °C under a nitrogen atmosphere. The field emission scanning electron microscopy (SEM) was performed on a JSM-6390. Powder X-ray diffraction (PXRD) was conducted on a PANalytical X'Pert Pro diffractometer with a Cu K_{α} X-ray source (λ = 0.154 nm). Ultraviolet-visible (UV-Vis) diffuse reflectance spectroscopy (DRS) was carried out on an UH4150 spectrophotometer with an integrating sphere mode. Photoluminescence (PL) spectroscopy measurement was conducted on a F-4600 FL Spectrophotometer. Transmission electron microscopy (TEM) was performed on a FEI Tecnai G2 Sphera microscope. Surface areas and pore size distributions were calculated from nitrogen absorption and desorption at 77 K using a micromeritics ASAP2020 HD88 Surface Area and Porosity Analyzer. Water contact angle measurements were performed with COFs film samples on a JC2000C instrument. Electrochemical Mott-Schottky curves and impedance spectroscopy were performed on a CHI-760E electrochemical workstation equipped with a three-electrode system using a glassy carbon electrode as working electrode, an Ag/AgCl electrode as the reference electrode, and a platinum wire as the counter electrode. The measurements were carried out in a 0.2 M sodium sulfate electrolyte solution. Femtosecond transient absorption spectroscopy was performed with a femtosecond Ti:sapphire regenerative amplified laser system (Spectra Physics, Spitfire-Pro) and a Helios-model ultrafast system. Structural modeling and theoretical calculations were carried out using the Materials Studio 7.0. The predicted structures with eclipsed (AA) and staggered (AB) stacking models were firstly optimized in geometry optimizations by the Forcite module, after which the simulated PXRD patterns were determined by the Reflex module. The Pawley refinement of the experimental PXRD was conducted by the Reflex module. The theoretical calculations on density of states (DOS), orbitals and electrostatic potentials were performed on the Forcite-predicted structures by the DMol3 model using GGA and PBE function.

2. Synthesis of 4,4'-(5,5-dioxidodibenzo[*b*,*d*]thiophene-3,7-diyl) dibenzaldehyde (**M2**)

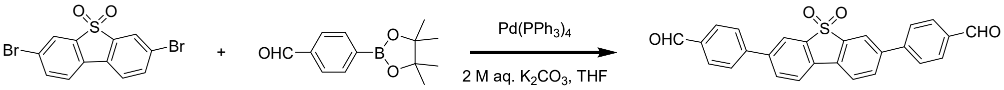

4-Formylbenzeneboronic acid pinacol ester (3.23 g, 13.92 mmol), 3,7-dibromodibenzo[*b*,*d*]thiophene-5,5-dioxide (1.3 g, 3.48 mmol), $Pd(PPh_3)_4$ (160.86 mg, 0.139 mmol) were added into a 250 mL three-mouth round bottom flask. After performing three times of nitrogen replacement, 80 mL THF and 20 mL K_2CO_3 (2 M) were added as solvents. The reaction mixture was degassed through three freeze-pump-thaw cycles, and heated at 68 °C in a N_2 atmosphere for 24 hours. Then, the mixture was cooled to room temperature and extracted with dichloromethane (DCM). The collected organic phase was washed three times with water, dried over Na_2SO_4, and evaporated off the solvent. Afterward, the residue was loaded onto a silica column and eluting with an eluent gradually changing from petroleum ether (PE), to PE/DCM-mixed solvent, and finally DCM, affording the product as a white solid (1.0 g, 68% yield).

^1H NMR (400 MHz, *DMSO-d$_6$*) δ: 10.10 (s, 2H), 8.51 (s, 2H), 8.42 (s, 2H), 8.29 (s, 2H), 8.14 (d, *J* = 8.2 Hz, 4H), 8.06 (s, 4H).

3. Synthesis of 3,7-bis(4-((*E*)-(phenylimino)methyl)phenyl)dibenzo[*b*,*d*] thiophene-5,5-dioxide (**DBTSO-imine**)

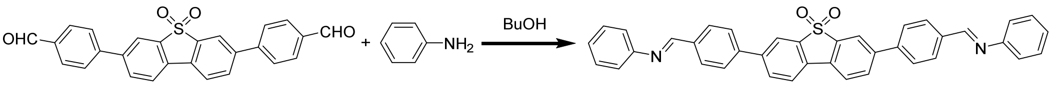

M2

DBTSO-imine

Aniline (93.13 mg, 1mmol) was added to a suspension of **M2** (21.22 mg, 0.05

mmol) in 2 mL of n-butanol. The reaction container was sealed and heated at 120 °C overnight, then cooled down to room temperature. The product was precipitated from the reaction mixture during the reaction, and thus collected by filtration after the reaction. After washed with ethanol many times and dried, the product was obtained in a white solid with a yield of 91.2%.

^{1}H NMR (400 MHz, *$CDCl_3$*) δ：8.54 (s, 2H), 8.13 (s, 2H), 8.07 (d, J=8.0Hz, 4H), 7.94 (s, 4H), 7.78 (d, *J* = 8.0 Hz, 4H), 7.43 (t, J=8.0Hz, 4H), 7.29 (s, 4H).

4. Supporting figures and tables

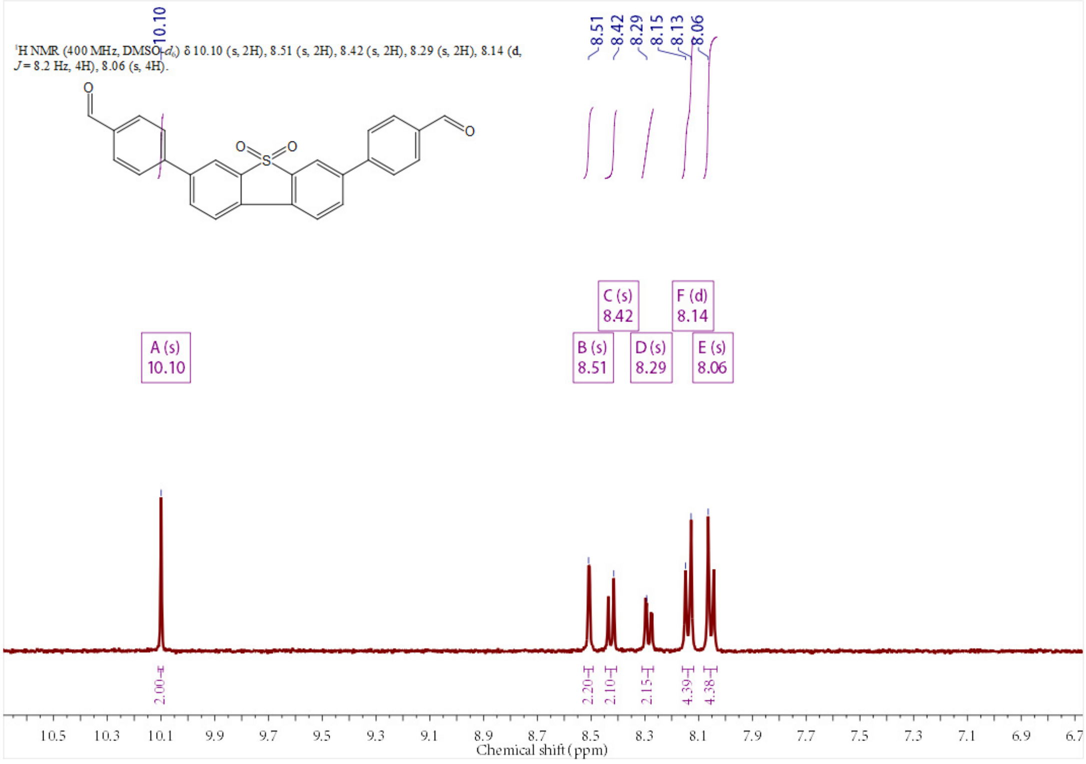

^1H NMR (400 MHz, DMSO-d_6) δ 10.10 (s, 2H), 8.51 (s, 2H), 8.42 (s, 2H), 8.29 (s, 2H), 8.14 (d, J = 8.2 Hz, 4H), 8.06 (s, 4H).

Fig. S1 ^1H NMR of **M2** in DMSO-d_6.

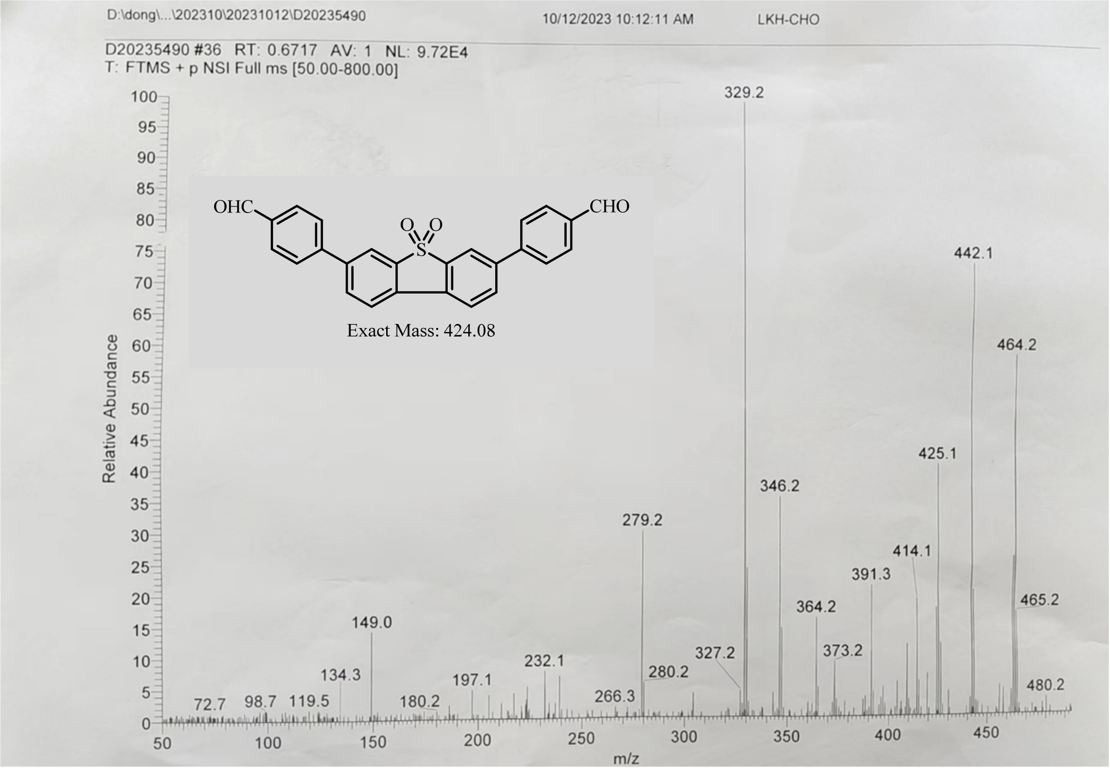

Fig. S2 Dart mass spectroscopy of **M2**.

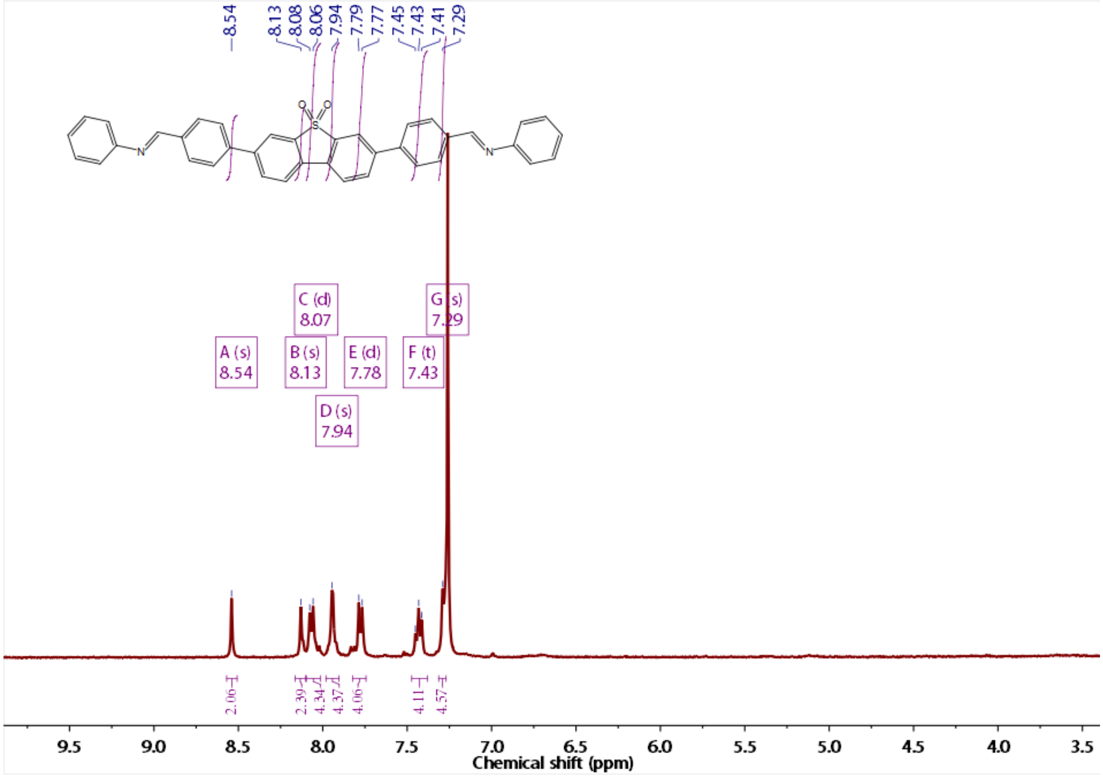

Fig. S3 ^{1}H NMR of **DBTSO-imine** in $CDCl_3$.

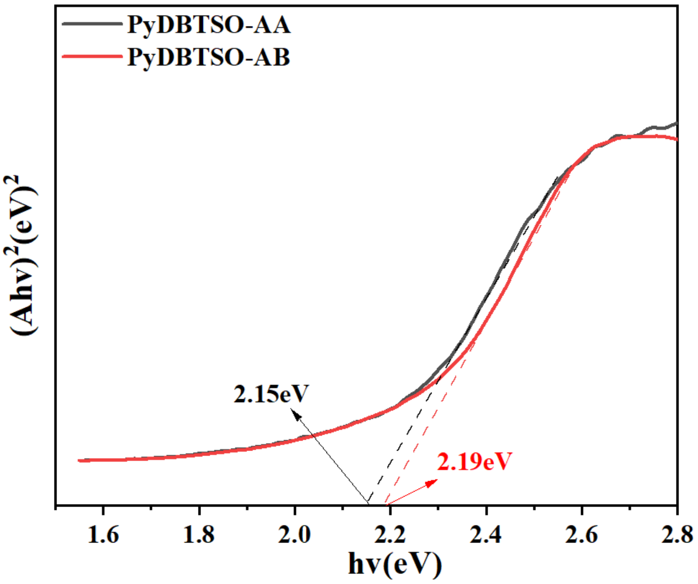

Fig. S4 Tauc plots of **PyDBTSO-AA** and **PyDBTSO-AB**.

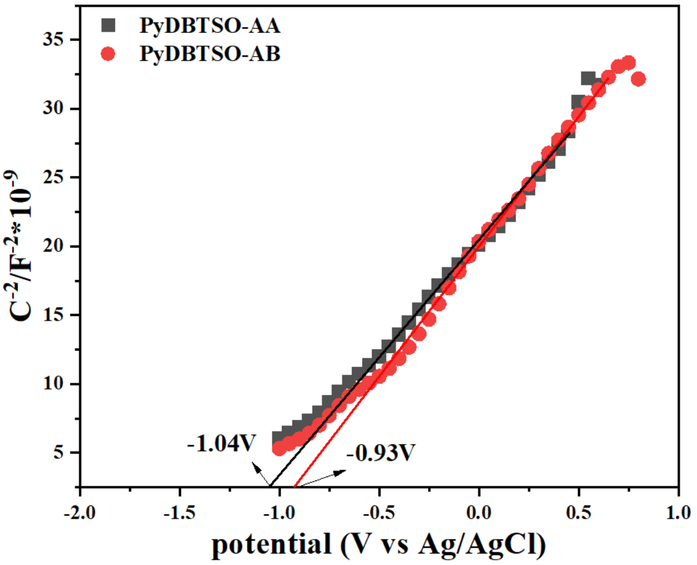

Fig. S5 Mott-Schotty curves of **PyDBTSO-AA** and **PyDBTSO-AB**.

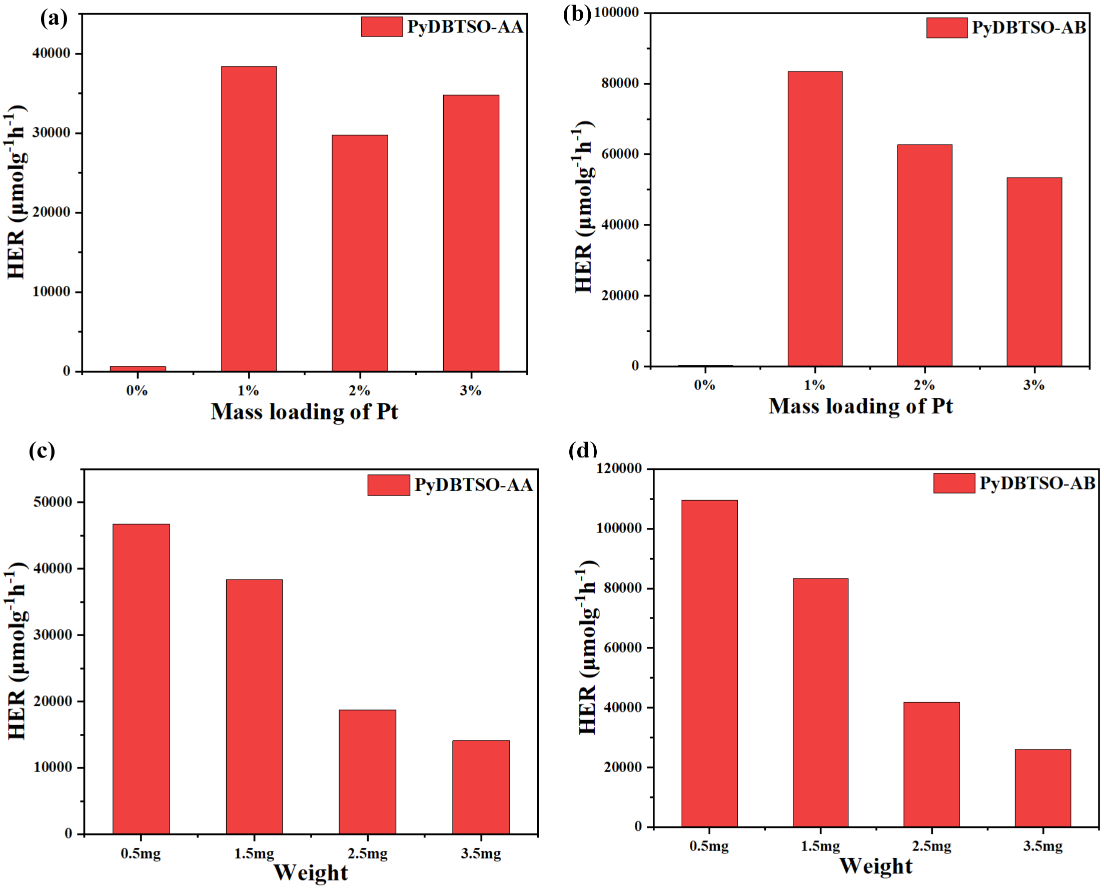

Fig. S6 Hydrogen evolution rate of **PyDBTSO-AA** and **PyDBTSO-AB** under different mass loadings of Pt co-catalyst and photocatalyst.

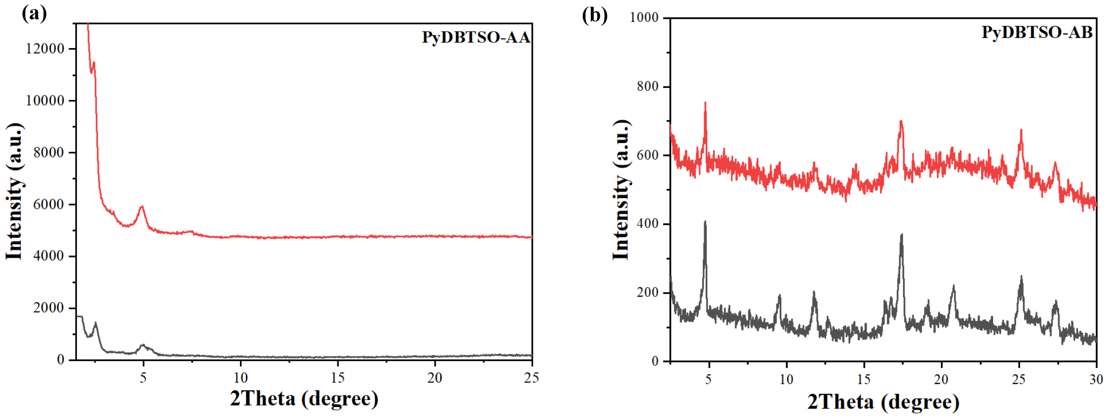

Fig. S7 (a) PXRD pattern of as-synthesized (black) and after long-term photocatalysis (red) of (a) **PyDBTSO-AA** and (b) **PyDBTSO-AB**.

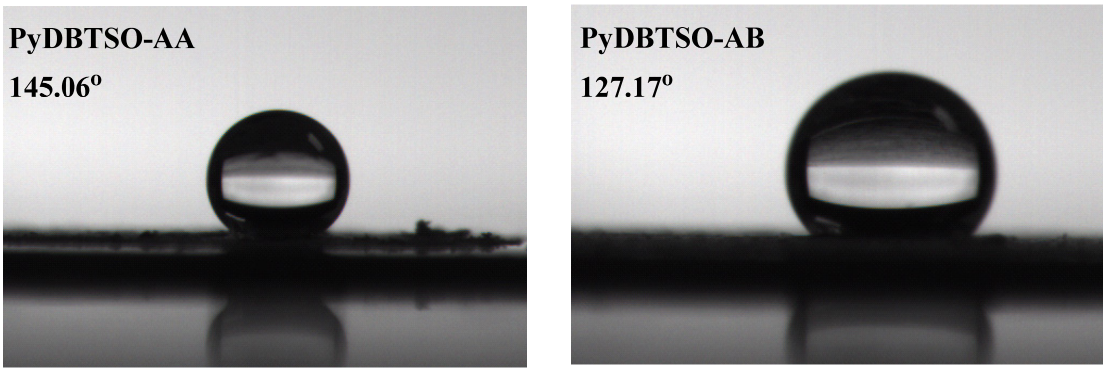

Fig. S8 Water contact angle of **PyDBTSO-AA** and **PyDBTSO-AB**.

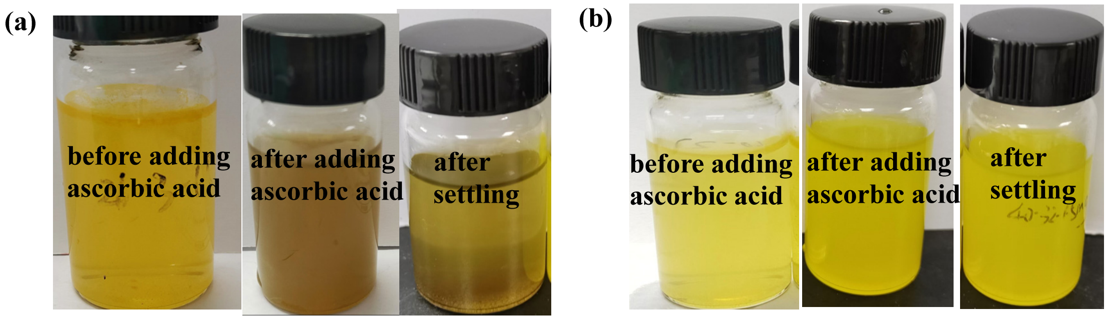

PyDBTSO-AA

PyDBTSO-AB

Fig. S9 (a) Photos of a **PyDBTSO-AA** dispersion before and after adding ascorbic acid, then settling for several hours. (b) Photos of a **PyDBTSO-AB** dispersion before and after adding ascorbic acid, then settling for several hours.

Table S1 Deconvoluted components of the fluorescence decay of **PyDBTSO-AA** and **PyDBTSO-AB** monitored at 420 nm

Samples	τ_1 (ns)	τ_2 (ns)	A_1 (%)	A_2 (%)	τ_{avg} (ns)
PyDBTSO-AA	0.41	3.02	77.20	22.80	1.01
PyDBTSO-AB	0.43	2.09	65.89	34.11	1.00

Table S2 Comparison of photocatalytic hydrogen-production performance of organic semiconductor photocatalysts

Material Type	Photocatalyst (amount)	Cocatalyst	Irradiation condition	Sacrificial reagent	HER mmol $g^{-1}h^{-1}$	Reference
Vinylene-linked COFs	ZVCOF-1 (1 mg)	1wt% Pt	300W Xe lamp λ >420 nm	0.1 M AA	288.8	J. Am. Chem. Soc. 2023, 145, 25222−25232.
	BTH-3 (5 mg)	8wt% Pt	300W Xe lamp λ >420 nm	0.1 M AA	15.1	Nat. Commun. 2022, 13, 100.
	TP-COF (5 mg)	8wt% Pt	300W Xe lamp λ >420 nm	10 vol.%TEOA	29.12	Sci China Mater. 2023, 66, 2283-2289
	TCDA-COF (5 mg)	1wt% Pt	300W Xe lamp λ >420 nm	0.1 M AA	70.8	J. Am. Chem. Soc. 2023, 145, 8364-8374
	v-2D-COF-NO1 (2 mg)	4.8wt% Pt	300W Xe lamp λ >400 nm	0.1 M TEOA	1.97	J. Am. Chem. Soc. 2022, 144, 13953-13960
Keto-enamine-linked COFs	S2-TP COF (2 mg)	3 wt% Pt	LED source λ >420 nm	0.1 M AA	14.35	Chem. Sci. 2024,

	Macro TpBpy (5 mg)	8 wt% Pt	300W Xe lamp λ >420 nm	0.1 M TEOA	4.88	Chem. Mater. 2024, 36, 8330-8337
	HKUST-1/1TpPa-1 (10 mg)	3 wt% Pt	300W Xe lamp λ >420 nm	0.03M AA	10.5	ChemSusChem. 2024, 17,e202400987
	COF-OH-3 (5 mg)	1 wt% Pt	300W Xe lamp λ >420 nm	0.1 M AA	9.89	J. Mater. Chem. A, 2022, 10, 24620-24627
	FS-COF (5 mg)	3.8 wt% Pt	300W Xe lamp λ >420 nm	0.1 M AA	10.1	Nat. Chem. 2018, 10, 1180-1189
	TP-BDDA COF (10 mg)	3 wt% Pt	300W Xe lamp λ >420 nm	10 vol.%TEOA	0.32	J. Am. Chem. Soc. 2018, 140,1423-1427
Imine-linked COF	PyAl-TpbAm-COF (5mg)	3wt% Pt	350W Xe lamp λ >420 nm	0.1 M AA	2.1	J. Mater. Chem. A, 2024, 12, 227–232.
	Py-hCOF (5 mg)	3wt% Pt	350W Xe lamp λ >420 nm	0.1 M AA	44.2	Chem. Sci., 2024, 15, 20002

	BTT-OH	3wt% Pt	300W Xe lamp λ >420 nm	AA	5.96	ACS Catal. 2024, 14, 11262-11272
	ZnP-Tt (2 mg)	3wt% Pt	300W Xe lamp λ >420 nm	BIH	11.1	Angew. Chem. Int. Ed. 2024, e202418319
	Py-CITP-BT-COF (20 mg)	5wt% Pt	300W Xe lamp λ >420 nm	0.1 M AA	8.86	Angew. Chem. Int. Ed. 2020, 59, 16902-16909
	TAPFy-PhI COF (10 mg)	1wt% Pt	300W Xe lamp λ >420 nm	0.1 M AA	2.72	ACS Appl. Mater. Interfaces.2023, 15,20310-20316
	TtaTfa (3 mg)	3.8wt% Pt	300W Xe lamp λ >420 nm	0.1 M AA	20.70	Angew. Chem. Int. Ed. 2021, 60, 19797-19803
Linear Conjugated Polymers	THTDB-4 (2 mg)	3wt% Pt	300W Xe lamp λ >420 nm	0.1 M AA	28.78	J. Colloid Interface Sci. 2024, 661, 333–344.
	DB-Th (2 mg)	no	300W Xe lamp λ >420 nm	0.5 M AA	334.5	Chem. Eng. J. 2023, 473, 145359

	PDBTSO-T\ (10 mg)	3wt% Pt	300W Xe lamp λ >300 nm	1 M AA	147	Appl. Catal. B. 2022, 307, 121144
	P(BDT-DBTSO$_{79}$) (3.5 mg)	3wt% Pt	300W Xe lamp λ >420 nm	33 vol.%TEA	119.3	Chin. J. Chem. 2022, 40,2457-2467
Conjugated Microporous Polymers	Py-DE-2F (2 mg)	1wt% Pt	300W Xe lamp λ >420 nm	0.5 M AA	66.0	J. Colloid Interface Sci. 2025, 683, 111-121.
	DBC-BTDO-2 (10 mg)	no	300W Xe lamp λ >300 nm	1 M AA	214.43	Chem. Eng. J. 2023, 459, 141553.
	PyDTDO-3 (10 mg)	no	300W Xe lamp λ >420 nm	1 M AA	16.32	Chem. Sci. 2020, 12, 1796-1802
	Py-TP-BDTO (5 mg)	3wt% Pt	300W Xe lamp λ >300 nm	1 M AA	331.37	ACS Catal. 2023, 13, 204-212